Quantum Phase Diffusion in a Small Underdamped Josephson Junction

H. F. Yu, X. B. Zhu, Z. H. Peng, Ye Tian, D. J. Cui, G. H. Chen, D. N. Zheng, X. N. Jing, Li Lu, S. P. Zhao, and Siyuan Han

Phys. Rev. Lett. **107**, 067004 — Published 3 August 2011

DOI: 10.1103/PhysRevLett.107.067004

Quantum Phase Diffusion in a Small Underdamped Josephson Junction

H. F. Yu, X. B. Zhu, Z. H. Peng, Ye Tian, D. J. Cui, G.
H. Chen, D. N. Zheng, X. N. Jing, Li Lu, and S. P. Zhao
Beijing National Laboratory for Condensed Matter Physics,
Institute of Physics, Chinese Academy of Sciences, Beijing 100190, China

Siyuan Han
Department of Physics and Astronomy,
University of Kansas, Lawrence, Kansas 66045, USA

Abstract

Quantum phase diffusion in a small underdamped Nb/AlO_x/Nb junction (~ 0.4 μm^2) is demonstrated in a wide temperature range of 25-140 mK where macroscopic quantum tunneling (MQT) is the dominant escape mechanism. We propose a two-step transition model to describe the switching process in which the escape rate out of the potential well and the transition rate from phase diffusion to the running state are considered. The transition rate extracted from the experimental switching current distribution follows the predicted Arrhenius law in the thermal regime but is greatly enhanced when MQT becomes dominant.

PACS numbers: 74.50.+r, 05.40.-a, 85.25.Cp

Classical and quantum diffusion of Brownian particles in titled periodic potential plays a fundamental role in the dynamical behavior of many systems in science and engineering [1–16]. Examples include current biased Josephson junctions [1–9], colloidal particles in arrays of laser traps [10, 11], cold atoms in optical lattice or Bose-Einstein condensates [12–14], and various biology-inspired systems known as Brownian motors (molecular motors or life engines), which receive considerable attention in physics [15] and chemistry [16]. Because of the design flexibility, manufacturability, and controllability Josephson junctions provide an excellent testbed for making quantitative comparison of experimental data with theoretical predictions and unraveling possible new physics in the tilted periodic potential systems.

The dynamics of a current biased Josephson junction can be visualized as a fictitious phase particle of mass C moving in a tilted periodic potential $U(\varphi) = -E_J(i\varphi + \cos\varphi)$. Here, C is junction capacitance, $i = I/I_c$ is the junction's bias current normalized to its critical current, the phase particle's position φ is the gauge invariant phase difference across the junction, and $E_J = \hbar I_c/2e$ is the Josephson coupling energy with e and $\hbar$ being the electron charge and Planck's constant, respectively. Previous experiments using Josephson junctions have identified three distinctive dynamical states, as shown schematically in Fig. 1. In the first state, the phase particle is trapped in one of the metastable potential wells and undergoes small oscillation around the bottom of the well with plasma frequency ω_p. Due to thermal and/or quantum fluctuations the particle has a finite rate Γ_1 escaping from the trapped state. The escape rate becomes significant when the barrier height ΔU is not much greater than k_BT or $\hbar\omega_p$, where k_B is the Boltzmann constant and T denotes the temperature, respectively. After the particle *escapes* from the initial well, depending on the energy gain $\delta U = \Phi_0 I$ (Φ_0 being the flux quantum) and the loss E_D due to damping (c.f. Fig. 1), it could

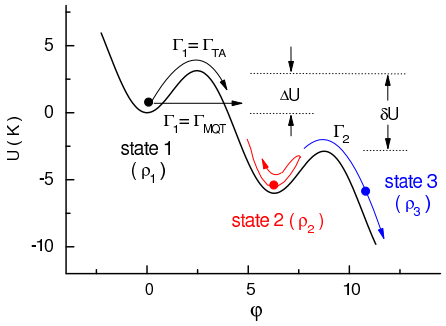

FIG. 1: (Color online) Phase particle in the trapped, diffusion, and running states (denoted by $n = 1, 2, 3$, respectively) with occupation probability ρ_n in a tilted washboard potential.

enter either the second dynamical state called phase diffusion (PD) or the final running state. In the former case as the bias current I is increased further the particle will eventually make a transition, characterized by a rate constant Γ_2, to the running state. While escape from the trapped state to PD is difficult to detect transition to the running state is signaled by a sudden jump in the dc voltage of the junction (called *switching*) and thus can be readily captured in real time by increasing I continuously from zero until a switching occurs [17].

The fundamental importance of understanding PD has stimulated many studies in recent years. However, experimental studies were focused mostly on the classical regime where thermal activation (TA) is the dominant escape mechanism and thermal fluctuation governs the PD process [1–9]. On the other hand, in the quantum regime where macroscopic quantum tunneling (MQT) dominates, one expects that quantum fluctuation induced tunneling will play an important role in the PD process and subsequent transition to the running state thus the term quantum PD (QPD) has been coined in the literature [15, 18–20]. However, although theoretical progress of QPD in overdamped systems has been remarkable over recent years [18, 19] the situation is so far much less clear for underdamped systems [15, 20].

In this work, we demonstrate QPD in a small underdamped Josephson junction over a wide temperature range of 25 mK to 140 mK. To contrast QPD with classical PD, we use two Nb-AlO_x-Nb trilayer junctions of different sizes (see Table I) having $T_0 \ll T_{cr}$ and $T_0 \gg T_{cr}$, respectively. Here, T_0 is the temperature above which PD occurs and T_{cr} is the classical-to-quantum crossover temperature below which MQT dominates. One of the hallmarks of PD in underdamped junctions

TABLE I: Parameters of two Nb/AlO_x/Nb junctions S and L used in this work. R_N is normal-state resistance obtained from I-V curves. I_c, C, and R for L are determined from fits to experiment using TA and MQT theories below 450 mK and Monte Carlo simulations above it. Those for S are obtained considering its R_N ratio to L (Note a slightly larger R chosen to have a better fit). See the text for details.

Junction	Area[a] (μm^2)	R_N(kΩ)	I_c(nA)	C(fF)	R(Ω)	T_{cr}(mK)	T_0(mK)
S	0.39	15.1	122	19.6	1800	140	< 25
L	1.54	3.84	480	77	315	125	~450

[a]Estimated for L from fitted C and a specific capacitance of 50 fF/μm^2. The value for S is obtained via its R_N ratio to L. Nominal areas for junctions S and L were 0.52 and 1.61 μm^2, respectively.

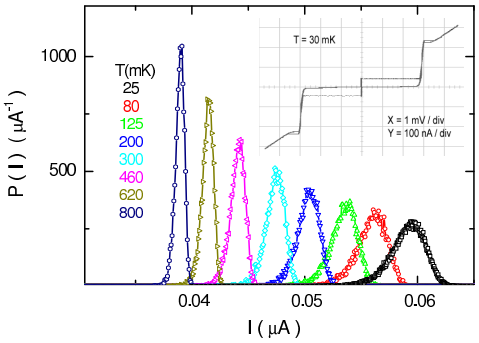

FIG. 2: (Color online) Experimentally measured $P(I)$ of junction S at some temperatures indicated. Inset shows the I-V trace of the junction at 30 mK.

is the narrowing of the width σ of switching current distribution $P(I)$ as temperature increases [5–8]. This is observed clearly in the measured $\sigma(T)$ of the larger junction L above $T_0^L \simeq 450$ mK $\gg T_{cr}^L$, which indicates that PD in this case is classical in nature. In sharp contrast, for the smaller junction S the width σ continues to increase as temperature decreases to the lowest value of 25 mK. When plotted in semi-logarithmic scale σ vs. T shows a clear increase of slope around $T_{cr}^S = 140$ mK, pointing to a change from classical PD to QPD. We will extract the transition rate Γ_2 directly from the experimental results and show that QPD is fundamentally different from classical PD.

Two Nb/AlO$_x$/Nb junctions used in this study were fabricated *on the same chip* with nominal areas of 0.52 and 1.61 μm^2 for junctions S and L, respectively. Compared with previous works reported in Refs. [5] and [6], where dc SQUIDs were used to tune I_c, our approach kept I_c/C constant. This unique approach is essential to extend PD to the quantum regime. Since $T_{cr} = \hbar\omega_p[(1 + 1/4Q^2)^{1/2} - 1/2Q]/2\pi k_B \sim \hbar\omega_0/2\pi k_B$ scales with the plasma frequency $\omega_p = \omega_0\left(1 - i^2\right)^{1/4}$, where $\omega_0 = (2\pi I_c/\Phi_0 C)^{1/2}$ and $Q = \omega_p RC$ (R being junction's damping resistance), T_{cr} is approximately independent of the junction sizes as long as they are fabricated from the same trilayer. On the other hand, T_0 can be reduced by making smaller junctions therefore we are able to tune T_0 and T_{cr} independently to meet the condition $T_0 \ll T_{cr}$ required for observing QPD [21].

Figure 2 shows the measured $P(I)$ from 25 to 800 mK for junction S with its I-V curve at 30 mK displayed in the inset. In our experiment, $P(I)$ was measured by the time-of-flight technique [8, 22] with $di/dt = 110$/sec for sample S and 163/sec for sample L. Each measured $P(I)$ consisted of 50000 switching events. In Fig. 3, we plot σ and the mean I_s of $P(I)$ versus temperature (symbols)

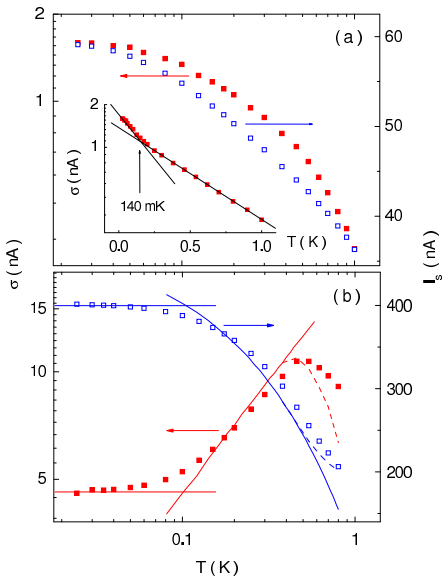

FIG. 3: (Color online) (a) Width σ and mean I_s of experimental $P(I)$ of junction S (symbols). (b) Corresponding data of junction L. Solid lines in (b) are calculated from TA and MQT theories while dashed lines from Monte Carlo simulations considering thermal PD [5, 8]. Inset shows σ of junction S plotted in semi-logarithmic scale. Two solid lines are guides to the eye displaying a slope turning near T_{cr}^S = 140 mK.

for junction S in (a) together with those of junction L in (b). For junction L the measured $\sigma(T)$ shows the familiar classical PD started at temperature $T_0^L \simeq 450$ mK well above T_{cr}^L = 125 mK. The solid lines in (b) are calculated according to the TA [23] and MQT [24] rate formulas using the parameters listed in Table I. The dashed lines are from Monte Carlo simulations considering thermal fluctuation and PD [5, 8]. In contrast to junction L the observed σ for junction S in Fig. 3(a) shows a monotonic decrease with increasing temperature, indicating that PD occurred in the entire temperature range of the experiment. Furthermore when plotting the data in semi-logarithmic scale as shown in the inset of Fig. 3 we notice a distinctive slope decrease around T_{cr}^S = 140 mK from MQT to TA regimes. Such a decrease can be easily understood since TA causes σ to increase with increasing T which partially cancels the effect of negative $(1/\sigma)d\sigma/dT$ due to PD.

To gain further insight and have a quantitative grasp on the effects of escape (from the trapped state to PD) and transition (from PD to the running state) on switching current distribution, regardless whether TA or MQT is the dominant mechanism, we set up the following master equation

according to the two-step transition model shown in Fig. 1:

$$\begin{cases} d\rho_1/dt = & = & -\Gamma_1\,\rho_1 \\ d\rho_2/dt = & = & \Gamma_1\,\rho_1 - \Gamma_2\,\rho_2 \\ d\rho_3/dt = & = & \Gamma_2\,\rho_2, \end{cases} \tag{1}$$

where ρ_n (n = 1, 2, 3) is probability of finding the phase particle in state n. Since $P(I) = d\rho_3/dI$, it follows straightforwardly that

$$\Gamma_2(I) = \frac{(dI/dt)P(I)}{1 - \int_0^I P(I')dI' - e^{-\frac{1}{dI/dt}\int_0^I \Gamma_1(I')dI'}}\,. \tag{2}$$

Eq. (2) shows that $\Gamma_2(I)$ can be extracted from measured $P(I)$ provided $\Gamma_1(I)$ is known, which is true in our experiment. Notice that in the limit of $\Gamma_2 \to \infty$, Eq. (2) leads directly to $\Gamma_1(I) = (dI/dt)P(I)/[1 - \int_0^I P(I')dI']$ which is identical to the result of Fulton and Dunkleberger [17] in which PD is absent. In the opposite limit of $\Gamma_2 \ll \Gamma_1$, the same expression is obtained with Γ_1 replaced by Γ_2: $\Gamma_2(I) = (dI/dt)P(I)/[1 - \int_0^I P(I')dI']$. These results mean that the much slower process plays the major role in determining $P(I)$, as expected. In the more general situation of $\Gamma_2 \sim \Gamma_1$, Eq. (2) enables one to separate the effect of Γ_2 on switching current distributions from that of Γ_1. The inverse procedure of computing $P(I)$ from Γ_1 and Γ_2 is given by:

$$P(I) = \frac{\Gamma_2}{(dI/dt)^2} e^{-\frac{1}{dI/dt}\int_0^I \Gamma_2 dI'} \int_0^I \Gamma_1 e^{-\frac{1}{dI/dt}\int_0^{I'} (\Gamma_1 - \Gamma_2)dI''} dI'. \tag{3}$$

Eqs. (2) and (3) thus allow us to quantitatively investigate the dependence of (Q)PD on bias current and the interplay between particle's escape and (Q)PD. In Fig. 4(a), we plot Γ_1 (solid lines) calculated using the parameters of junction S and Γ_2 (symbols) extracted from the measured $P(I)$ using Eq. (2). It can be seen that at T = 800 mK, Γ_1 is several orders of magnitude greater than Γ_2. The measured $P(I)$ is therefore entirely determined by Γ_2. As temperature decreases, Γ_1 is seen to progressively approach Γ_2.

Having clearly established that PD occurs in both classical and quantum regimes in junction S, we now use the data in Fig. 4(a) to further demonstrate the key difference between classical PD and QPD. In Fig. 4(b), we plot Γ_2 versus $1/T$ at three bias currents (thus fixed potentials) of 48, 52, and 56 nA, which shows distinct features below and above T_{cr}^S. While the data above T_{cr}^S follow the straight lines, indicating that Γ_2 in the classical regime obeys the Arrhenius law Γ_2 displays a much weaker $1/T$ dependence at below $T \ll T_{cr}^S$. We note that similar behavior in the classical regime was discussed previously by Vion *et al.* [3] for overdamped system where the diffusive

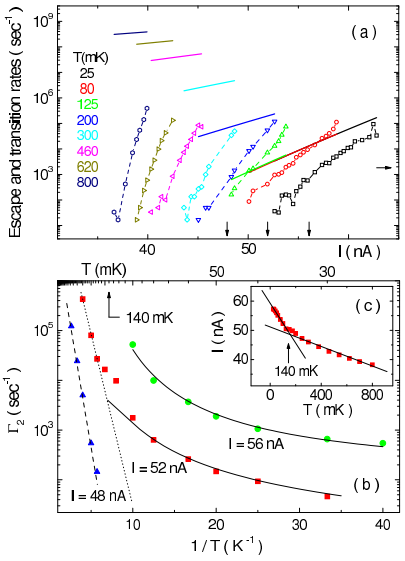

FIG. 4: (Color online) (a) Transition rate Γ_2 (symbols) and escape rate Γ_1 (solid lines) of junction S at some typical temperatures. (b) $\Gamma_2 \sim 1/T$ at three fixed currents as indicated by the vertical arrows in (a). Dashed and dotted lines are fits displaying the Arrhenius law. (c) $I \sim T$ for fixed $\Gamma_2 = 2000$ sec^{-1} as indicated by a horizontal arrow in (a). Solid lines in (b) and (c) are guides to the eye.

particle is considered to overcome an effective dissipation barrier. In that case, the transition rate from PD to the running state, which retains the familiar Kramers form, was derived. Fitting the data above T_{cr}^S using $\Gamma_2 = a\exp(-b/T)$, we obtain $a = 5.2 \times 10^7$ sec^{-1}, $b = 2.3$ K for $I = 48$ nA (dashed line) and $a = 3.3 \times 10^8$ sec^{-1}, $b = 1.7$ K for $I = 52$ nA (dotted line). The effective barrier b appears smaller as compared to the calculated barrier height ΔU of 2.68 and 2.46 K due to the motion of the diffusive particles, which is physically quite reasonable. These results indicate that in the thermal regime a dissipation-barrier description is also applicable to PD in underdamped junctions.

Machura *et al.* recently investigated the diffusion problem of overdamped particles using the Smoluchowski equation incorporating quantum fluctuations [19]. They found that the particle's average velocity $\langle v \rangle$ increases with increasing temperature and quantum effects always assist the particle to overcome barriers leading to a larger $\langle v \rangle$ than that in absence of quantum fluctuations. Because in our underdamped junction the dc voltage, which is proportional to $\langle v \rangle$, produced by PD is too low to be detected directly [25], it can nevertheless be expected that a larger $\langle v \rangle$ would result in a larger Γ_2 since the increased kinetic energy makes transitions to the running state easier. For this reason, the data in Fig. 4(b) are consistent with the theoretical prediction since extrapolating

Γ_2 from the classical to the quantum regime would lead to rates that are much lower than the experimental data. Therefore, the much weaker $1/T$ dependence of Γ_2 below T_{cr}^S, in a stark contrast to the Arrhenius behavior above T_{cr}^S, manifests the *quantum* nature of the diffusion process at $T < T_{cr}^S$.

In Fig. 4(c) we plot I versus T for a constant $\Gamma_2 = 2000$ sec^{-1}, which again shows a distinctive change of slope around T_{cr}^S similar to that of σ. The approximate linear $I - T$ dependence above T_{cr}^S can be qualitatively explained. In the absence of thermal fluctuations transition from PD to running state is expected to occur deterministically at I_0 where $\delta U_0 = (h/2e)I_0 = E_D$. For $T > 0$ the phase particle will exit the PD state prematurely because the particle on average acquires an additional thermal energy of $\sim k_B T$. Thus the condition for transition out of PD needs to be revised to $\delta U + k_B T = E_D$. Assuming junction's damping, and thus E_D, saturates at low T we obtain $(h/2e)I = E_D - k_B T$. The predicted slope $|s| = 2ek_B/h \approx 7$ nA/K is comparable to the experimental value of 15 nA/K in the thermal regime in Fig. 4(c), which is quite reasonable considering the simplicity of the model. Below T_{cr}^S, however, the measured $|s|$ increased to about 68 nA/K, about an order of magnitude greater than $2ek_B/h$ which remains unexplained.

In conclusion, QPD was demonstrated and systematically studied in a small underdamped Nb Josephson junction. Using junctions of different sizes fabricated on the same chip we were able to calibrate the relevant parameters of the small junction and at the same time extended QPD over a wide temperature range. We showed that σ decreases monotonically with increasing temperature and there is a distinctive change of slope at T_{cr} below and above which QPD and classical PD occur. We developed a two-step transition model with which the effects of escape rate Γ_1 (from the trapped state) and the transition rate Γ_2 (from PD to the running state) on switching current distributions can be separated and Γ_2 be determined from the measured $P(I)$ directly. It was found that Γ_2 vs. T at fixed bias current, and thus fixed potential landscape, follows the Arrhenius law in the case of classical PD. The most important finding was that for QPD, Γ_2 is exponentially higher than that expected for the classical PD and has a much weaker $1/T$ dependence. The similarities between the temperature dependence of Γ_1 and Γ_2 in underdamped Josephson junctions going from classical to quantum regimes were striking. We wish our experimental progress and advancement in data analysis will stimulate further theoretical and experimental studies of and lead to a better understanding of the quantum diffusion phenomena in underdamped tilted periodic potential systems.

We are grateful to H. Tang and Z. B. Su for helpful discussion and derivation of Eqs. (2) and

(3). We thank V. Patel, W. Chen, and J. E. Lukens for providing us with the samples used in this work. The work at the Institute of Physics was supported by NSFC (Grant No. 10874231) and 973 Program (Grant Nos. 2009CB929102 and 2011CBA00106). S. Han was supported in part by NSF Grant No. DMR-0325551.

[1] J. M. Martinis and R. L. Kautz, Phys. Rev. Lett. **63**, 1507 (1989).

[2] M. Iansiti *et al.*, Phys. Rev. B **39**, 6465 (1989).

[3] D. Vion *et al.*, Phys. Rev. Lett. **77**, 3435 (1996).

[4] Y. Koval, M. V. Fistul, and A. V. Ustinov, Phys. Rev. Lett. **93**, 087004 (2004).

[5] J. Männik *et al.*, Phys. Rev. B **71**, 220509(R) (2005).

[6] J. M. Kivioja *et al.*, Phys. Rev. Lett. **94**, 247002 (2005).

[7] V. M. Krasnov *et al.*, Phys. Rev. Lett. **95**, 157002 (2005).

[8] Shao-Xiong Li *et al.*, Phys. Rev. Lett. **99**, 037002 (2007).

[9] J. C. Fenton and P. A. Warburton, Phys. Rev. B **78**, 054526 (2008).

[10] M. Evstigneev *et al.*, Phys. Rev. E **77**, 041107 (2008).

[11] S. H. Lee and D. G. Grier, Phys. Rev. Lett. **96**, 190601 (2006).

[12] R. Gommers *et al.*, Phys. Rev. Lett. **100**, 040603 (2008).

[13] M. Schiavoni *et al.*, Phys. Rev. Lett. **90**, 094101 (2003).

[14] G. Tayebirad *et al.*, Phys. Rev. A **82**, 013633 (2010).

[15] P. Hänggi and F. Marchesoni, Rev. Mod. Phys. **81**, 387 (2009).

[16] G. S. Kottas *et al.*, Chem. Rev. **105**, 1281 (2005).

[17] T. A. Fulton and L. N. Dunkleberger, Phys. Rev. B **9**, 4760 (1974).

[18] J. Ankerhold, Europhys. Lett. **67**, 280 (2004).

[19] L. Machura *et al.*, Phys. Rev. E **73**, 031105 (2006).

[20] S. Denisov, S. Kohler and P. Hänggi, Europhys. Lett. **85**, 40003 (2009).

[21] In the case of dc SQUIDs we have fixed C thus $T_{cr} \propto \sqrt{E_J}$ which decreases also as I_c is reduced.

[22] H. F. Yu *et al.*, Phys. Rev. B **81**, 144518 (2010).

[23] H. A. Kramers, Physica (Utrecht) **7**, 284 (1940).

[24] A. O. Caldeira and A. J. Leggett, Phys. Rev. Lett. **46**, 211 (1981).

[25] No dc voltage signal within our measurement sensitivity ($\sim 0.5\,\mu$V) was detected for junction S before

switching.